MATERIALS PHYSICS AND MECHANICS RESEARCH ARTICLE

Submitted: December 3, 2025 **Revised: March 10, 2026** **Accepted: March 18, 2026**

Interpretation of macroscopic and microscopic optical properties of Sm^{3+} doped ZnF_2-PbO-B_2O_3 glass systems

B. Suresh [1], P. Naresh [2]✉, P. Sobhanachalam [3], N. Narasimha Rao [4], Ch. Rani [1], M. Srinivasa Reddy [5]

[1] Kallam Haranadha reddy Institute of Technology, Guntur, Andhra Pradesh, India

[2] VR Siddhartha School of Engineering, Siddhartha Academy of Higher Education (Deemed to be University), Vijayawada, Andhra Pradesh, India

[3] Lakireddy Bali Reddy College of Engineering, Mylavaram, Andhra Pradesh, India

[4] Krishna University Dr. MRAR College of PG Studies, Nuzvid, Andhra Pradesh, India

[5] Univ. College of Engineering and Technology, Acharya Nagarjuna University, Nagarjuna Nagar Andhra Pradesh, India

✉ nareshp6@rediffmail.com

ABSTRACT

The preparation and spectroscopic investigation of Sm_2O_3 doped ZnF_2–PbO–B_2O_3 glasses. XRD patterns confirmed their amorphous nature are reported. From measured densities, various physical parameters – including molar volume, optical band gap, refractive index, electronic polarizability and optical basicity were systematically evaluated and presented. Optical absorption spectra show well defined Sm^{3+} transitions from $^6H_{5/2} \rightarrow {}^6F_J$ where $J = {}^{11}/_2 - {}^1/_2$ levels. The optical band gaps are found to be minimal for the glass containing 2.0 mol. % Sm_2O_3. Judd-Ofelt analysis yielded $\Omega_2 > \Omega_4 > \Omega_6$ with bonding parameter δ highest at 2.0 mol. % Sm_2O_3, indicating a less covalent environment. Overall, the linear variation of physical and optical properties reflects the compositional role of Sm_2O_3. These results provide useful for potential laser-host applications.

KEYWORDS

borate glasses • Sm doped glasses • optical parameters • JO parameters • FTIR spectra • lead contained glasses

Citation: Suresh B, Naresh P, Sobhanachalam P, Narasimha Rao N, Rani Ch, Srinivasa Reddy M. Interpretation of macroscopic and microscopic optical properties of Sm^{3+} doped ZnF^2-PbO-B^2O^3 glass systems. *Materials Physics and Mechanics*. 2026;54(2): 70–82.
http://dx.doi.org/10.18149/MPM.5422026_6

Introduction

In view of many aspects including structure, stability, chemical durability, hosting the modifier up to a larger extent etc., B_2O_3 stands as a unique glass network former among the others like SiO_2, P_2O_5, As_2O_3, and GeO_2. Literature studies on borate glasses [1–8] explicitly demonstrate that the structure of pure borate glass is primarily built from trigonal planer BO_3 flat triangles embedded with boroxol rings (B_3O_6). In general, the bonding between boron and oxygen in the planar BO_3 unit is partially covalent with sp^2 hybridization and partially ionic with differences in electronegativity (oxygen becomes more electronegative than boron). In pure borate glass, boroxol ring is formed by three BO_3 triangles, which subsequently create three-dimensional networks with bridging oxygens (BOs) which causes to attain characteristics including presumably low density,

© B. Suresh, P. Naresh, P. Sobhanachalam, N. Narasimha Rao, Ch. Rani, M. Srinivasa Reddy, 2026.
Publisher: Peter the Great St. Petersburg Polytechnic University
This is an open access article under the CC BY-NC 4.0 license (https://creativecommons.org/li-censes/by-nc/4.0/)

high transparency in UV (ultraviolet) and IR (infrared) region, high thermal conductivity and lower electrical conductivity.

$PbO–B_2O_3$ has wider glass forming region ranging from 0.4 to 90 mol. % of PbO with stable phase separation. Adding PbO to B_2O_3 glasses significantly modifies their physical, optical and structural properties and also this modification is strongly compositional dependent. With low PbO concentrations up to ~ 20 mol. % plays a modifier role by breaking B–O–B linkages and encourages the conversion of BOs into non-bridging oxides (NBOs) by changing the boron atoms to tetragonal BO_4 (sp^3 hybridization) from trigonal BO_3 planer (sp^2 hybridization), which provides the pathway to increase the density and compactness of the glass [9], whereas with moderate PbO concentration up to ~ 40 mol. % [10] still plays a modifier role but with transition phase by producing more tetragonal BO_4 units and NBOs with separation of borate network which causes the decrease in connectivity and glass samples becomes less rigid. However, with more than 40 to 80 mol. % [11], PbO starts acts as a modifier by forming Pb–O–Pb linkages leading to the formation of pyramidal or square –planer PbO_4 structural units. Hence the network becomes weaker, creates a pathway to lower the glass transition temperature, and increases thermal expansion, electrical conductivity properties and refractive index. Despite of the above benefits, there are some handicaps like toxicity and environmental hazards that become expensive for processing and disposal.

When ZnF_2 is added to a binary composition like $PbO–B_2O_3$, it interacts with both borate and lead oxide units by introducing Zn^{2+} and F^- ions. Adding ZnF_2 [12,13] leads to the conversion of BO_3 units to BO_4 units and PbO into PbF_2 as follows:

$$Zn^{2+} + BO_3 \rightarrow Zn - O - BO_4,$$

$$ZnF_2 + PbO \rightarrow ZnO + PbF_2.$$

Moreover, ZnF_2 is added to $PbO–B_2O_3$, Zn^{2+} competes with Pb^{2+} for network modifier positions by replacing the Pb–O bonds with Zn–O bonds. Hence, Zn^{2+} acts as a modifier along with this it is also important to mention that modifying action is strongly based on the composition of the glass. The presence of two different network modifier ions Zn^{2+} and Pb^{2+} can disrupt the glass network by breaking B–O bonds and introducing NBOs, influencing the atomic packing, density and glass transition temperature [14,15]. Hence the optimal Zn/Pb ratio leads to a glass with adjustable properties that were essential for maintaining the durability of the glass sample. With these factors, we are motivated to choose the glass composition of 20 % ZnF_2–20 % PbO–60 % B_2O_3 system for the present study.

In the last few decades, lanthanide ion-doped glasses have drawn more attention due to the exhibition of well-defined sharp absorption/emission spectra due to 4f–4f intra-ion transitions, high quantum efficiency, up-conversion luminescence, local symmetry of lanthanide ions, which leads to the host glass matrix suitable as the best optical materials for the lasers, biosensing, optical amplifiers, radiation dosimetry, tunable light-emitting diodes (LEDs). Samarium is the sixth element in the lanthanide series with atomic number 62, electronic configuration $[Xe]4f^66s^2$. These $4f^6$ unpaired electrons are responsible for the distinct optical and magnetic properties. In general, Samarium exists in two oxidation states Sm^{2+} $[Xe]4f^6$ and Sm^{3+} $[Xe]4f^5$ among these, the second one usually plays a crucial role in the optical properties.

Nevertheless, it is important to mention that this fluoroborate system provides improved rare-earth ion solubility and favourable spectroscopic characteristics compared with conventional borate glasses, making it a promising host matrix for studying Sm^{3+} ion optical properties. In the present investigation, we have attempted to characterize the optical absorption of Sm^{3+} in zinc lead borate glasses mixed with different concentrations of Sm_2O_3 to get insight into the possible use of these glasses as laser hosts. The study is additionally intended to understand the relation between the macroscopic and microscopic optical properties and physical parameters.

Materials and Methods

The present studied glass samples had been prepared by adopting the melting and quenching method which is as similar as mentioned in our previous works [12,16]. Within the glass-forming region of system, the compositions are chosen for the present study is 20 ZnF_2 – (20–*x*)PbO – 60 B_2O_3: *x* Sm_2O_3 (with *x* = 0.5, 1.0, 1.5 and 2.0 all in ml. %). The detailed chemical composition of their codes is displayed in Table 1. Figure 1 depicts a schematic representation of the glass sample preparation process.

Table. 1. Composition of glass samples (all in mol. %)

Sample Code	ZnF_2	PbO	B_2O_3	Sm_2O_3
S_0	20.0	20.0	60.0	---
S_1	20.0	19.5	60.0	0.5
S_2	20.0	19.0	60.0	1.0
S_3	20.0	18.5	60.0	1.5
S_4	20.0	18.0	60.0	2.0

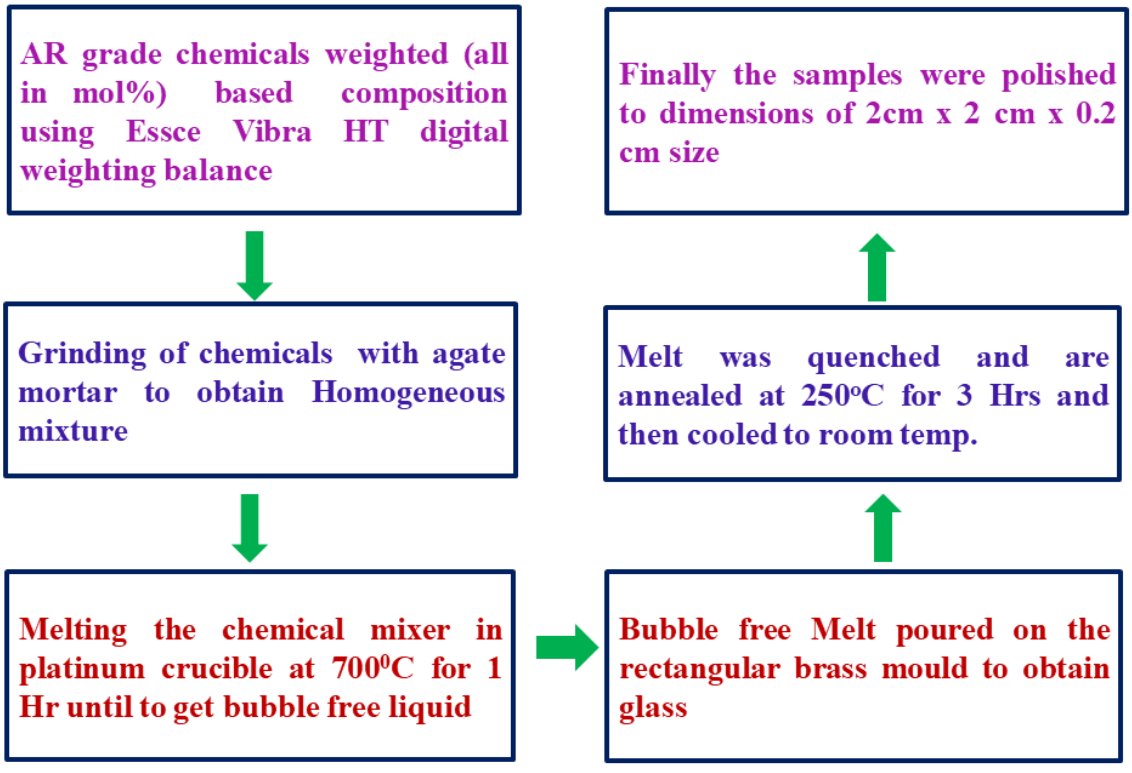

Fig. 1. Flow-chat of various steps involved in preparation of ZnF_2-PbO-B_2O_3:Sm_2O_3

The X-ray diffraction (XRD) patterns were recorded using the Philips PW 1830 X-ray diffraction spectrometer. The optical absorption spectra of samples acquired by using the JASCO V-670 UV-VIS spectrophotometer at room temperature in the wavelength range of 300–1800 nm. The infrared transmission spectra recorded by the Shimadzu IR Affinity-1S spectrophotometer by using KBr pellets in the 400–2000 cm^{-1} wavenumber region. The Vibra HT density kit is used for measuring the weights of the glass samples in air as well as in buoyant medium acetone. The refractive index of the glass samples measured using the Abbe refractometer using monochromatic wavelength 589.3 nm with mono-bromo naphthalene as the contact layer.

Results and Discussion

Using classical Archimedes' principle, densities have been computed, by measuring the weights of the samples in acetone and air using the equation:

$$\rho = \left(\frac{W_a}{W_a - W_l}\right)\rho_b, \quad (1)$$

where ρ is density of the sample, W_a and W_l are the samples weights in O-xylene and air, respectively, ρ_b is is density of the O-xylene. It was discovered that densities decreased as the quantity of dopant Sm_2O_3 in the glass matrix increased. Using these obtained densities various other significant parameters viz., molar volume (V_m), oxygen packing

Table 2. Physical parameters of Sm_2O_3 doped ZnF_2–PbO–B_2O_3 glasses

Property	Standard relation	Sample code				
		S_0	S_1	S_2	S_3	S_4
Density (ρ), g/cm³	$\rho = \left(\frac{W_a}{W_a - W_l}\right)\rho_b$	4.173	4.165	4.159	4.157	4.142
Avg. mol. weight ($\bar{M}$)	$\bar{M} = \sum X_i M_i$	107.09	107.72	108.35	108.97	109.60
Refractive index (n)	Experimental	1.685	1.723	1.735	1.742	1.757
Molar volume (V_m), cm³/mol	$V_m = \bar{M}/\rho$	25.66	25.86	26.05	26.21	26.46
Sm^{3+} ion concentration (N_i), ×10^{21} ions/cm³	$N_i = \frac{N_A x_i \rho}{\bar{M}}$	---	11.60	23.10	34.50	45.50
Inter ionic distance (r_i), Å	$r_i = \left[\frac{1}{N_i}\right]^{1/3}$	---	4.411	3.510	3.072	2.800
Polaron radius (r_p), Å	$r_p = \frac{1}{2}\left[\frac{\pi}{6N_i}\right]^{1/3}$	---	1.777	1.414	1.238	1.128
Reflection loss (R_L), ×10^{-2}	$R_L = \left[\frac{n-1}{n+1}\right]^2$	0.0650	0.0704	0.0722	0.0732	0.0753
Molar refraction (R_m)	$R_m = \left(\frac{n^2-1}{n^2+2}\right)V_m$	12.293	12.829	13.059	13.219	13.512
Molar electronic polarizability (α_m)	$\alpha_m = \frac{R_m}{2.52}$	4.878	5.091	5.182	5.245	5.361
Electronic polarization (α_e)	$\alpha_e = \frac{3(n^2-1)}{4\pi N_A(n^2+2)}$	1.899	1.967	1.987	1.999	2.025
Metallization criterion (M)	$M = 1 - \frac{R_m}{V_m}$	0.520	0.503	0.498	0.495	0.489
Energy gap (E_g), eV	$E_g = (\alpha\hbar\omega)^{1/2} = = C(\hbar\omega - E_o)$	1.620	1.599	1.593	1.589	1.581

density (OPD), polaron radius (R_p), inter–ion distance (R_i), and dopant-ion concentration (N_i) are estimated and presented in Table 2 along with used standard equations [17,18]. Table 2 shows that molar volume and Sm^{3+} ion concentration increase, whereas polaron radius and inter-ionic distance decrease with increasing the Sm_2O_3 content.

The absolute refractive index (*n*) at a specific wavelength of 589.3 nm was measured. The refractive index values for the studied samples were found ~ 1.68 to 1.76 following the increasing trend with increasing the Sm_2O_3 content. Using standard relations along with the measured densities and refractive indices, the physical parameters such as molar refraction, molar electronic polarizability, and metallization criteria were evaluated and same were systematically presented in Table 2. From Table 2, it is observed that molar refraction and molar electronic polarizability increase with increasing the Sm_2O_3 content, whereas the metallization criteria decrease with Sm_2O_3 content.

The diffraction patterns of all samples exhibited broad diffuse halos without any sharp crystalline peaks, confirming the amorphous nature of the glasses across the prepared compositional range. Since all compositions displayed similar amorphous diffraction features, only a representative XRD pattern corresponding to the S_4 sample (2.0 mol. % Sm_2O_3) has been presented in Fig. 2.

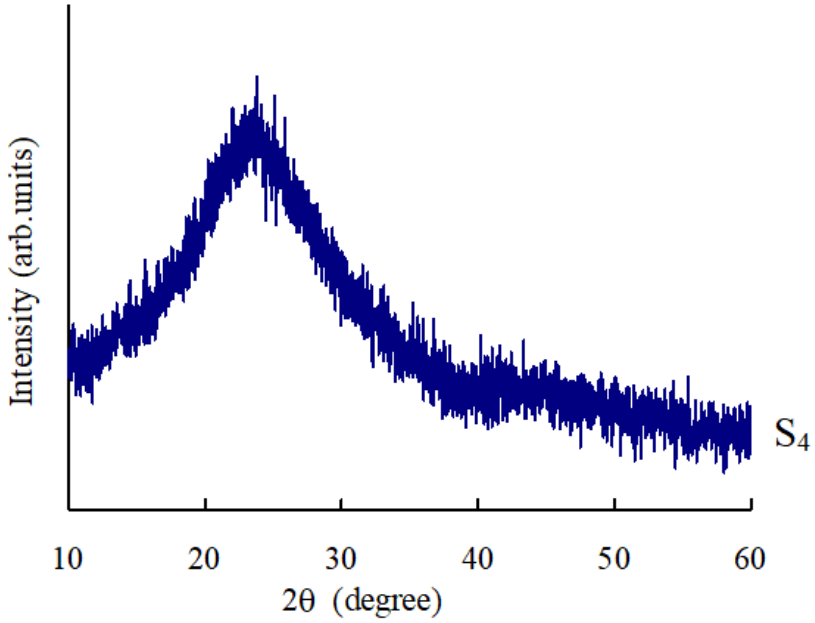

Fig. 2. X-ray diffraction pattern of ZnF_2–PbO–B_2O_3 glasses doped with 2.0 mol. % Sm_2O_3

The optical absorption spectra of Samarium doped ZnF_2–PbO–B_2O_3 glasses recorded at room temperature in the wavelength range 200–2000 nm is shown in Fig. 3. The spectra of S_1 samples exhibits the absorption bands with peak positions at about 935, 1070, 1224, 1367, 1364, and 1578 nm. Based on the literature [19,20], these observed bands are assigned due to $^6H_{5/2} \rightarrow {}^6F_{11/2}$, $^6F_{9/2}$, $^6F_{7/2}$, $^6F_{5/2}$, $^6F_{3/2}$, and $^6F_{1/2}$ transitions respectively. Other glass samples also exhibit peaks with a slight shift in band position which is expected due to the structural changes that take place in a sample by the compositional change. The details of the observed band positions for the samples are presented in Table 3.

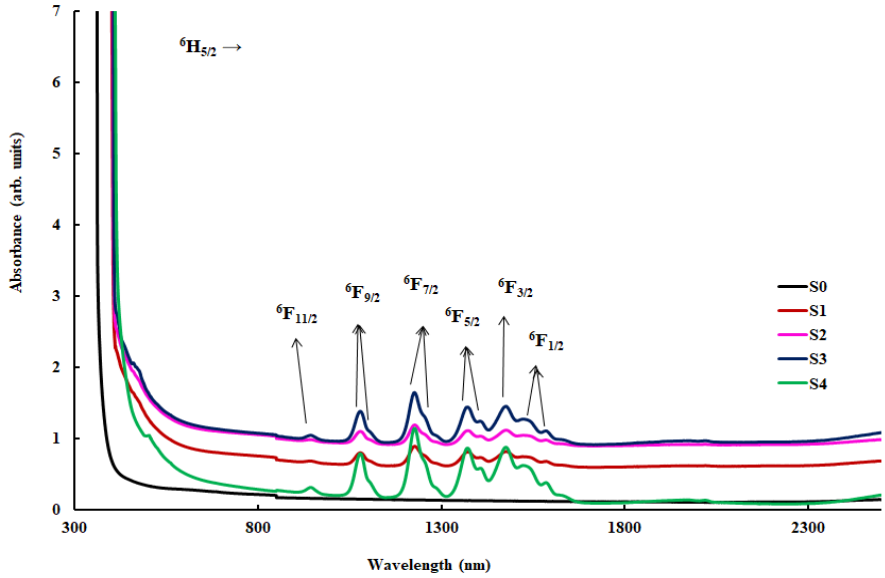

Fig. 3. Optical absorption spectra for ZnF_2–PbO–B_2O_3 glasses mixed with different concentration of Sm_2O_3

Table 3. Optical absorption data and band gaps of Sm_2O_3 doped ZnF_2–PbO–B_2O_3 glasses

	Glass				
	S_0	**S_1**	**S_2**	**S_3**	**S_4**
Cut-off wavelength, nm	361.5	380	406	407	409
$^6H_{5/2}\rightarrow{}^6F_{11/2}$	---	935	931	933	936
$^6H_{5/2}\rightarrow{}^6F_{9/2}$	---	1070	1073	1075	1076
$^6H_{5/2}\rightarrow{}^6F_{7/2}$	---	1224	1223	1224	1225
$^6H_{5/2}\rightarrow{}^6F_{5/2}$	---	1367	1365	1366	1368
$^6H_{5/2}\rightarrow{}^6F_{3/2}$	---	1394	1395	1397	1398
$^6H_{5/2}\rightarrow{}^6F_{1/2}$	---	1578	1579	1579	1580
Optical band gap E_o, eV	3.40	3.02	2.98	2.92	2.90

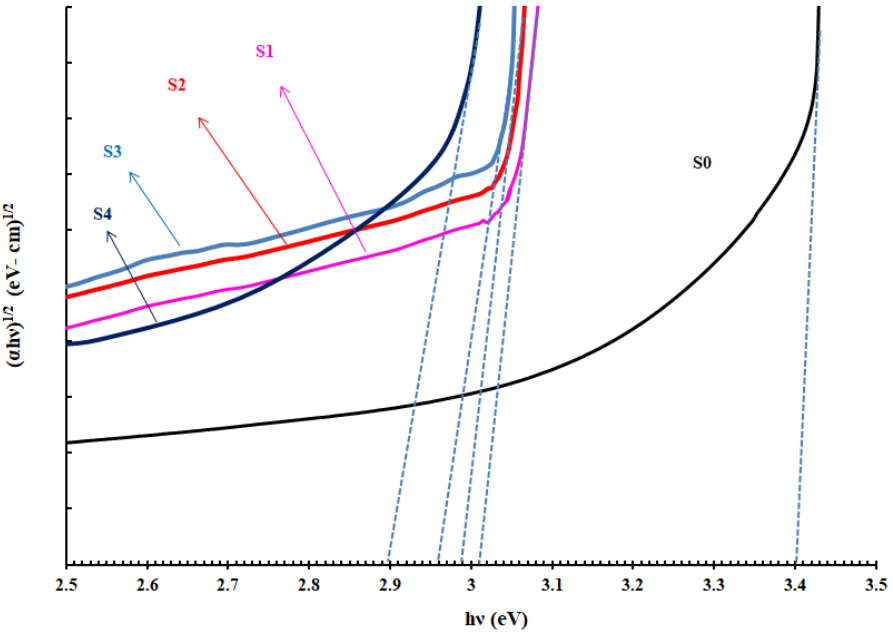

Fig. 4. Tauc plots between $(\alpha\hbar\omega)^{1/2}$ vs $\hbar\omega$ for ZnF_2–PbO–B_2O_3 glasses mixed with different concentration of Sm_2O_3

The optical band gap (E_o) of all the glasses is evaluated by drawing Tauc plots between $(\alpha\hbar\omega)^{1/2}$ vs $\hbar\omega$ (Fig. 4) as per Eq. (2) [12]:

$$E_g = (\alpha\hbar\omega)^{1/2} = C(\hbar\omega - E_o), \quad (2)$$

where $\hbar\omega$ is the photon energy, E_o is the optical band gap and C is a temperature independent constant related to the extent of the band tailing. The energy band gap of the samples is found to be the shrinkage with increasing the content of Sm^{3+} ion in the sample (Table 3), where X_i is the mol. % of the oxide compound,M_i is the molecular weight of the compound, ρ_b is the density of acetone, N_A is the Avogadro number, Z is the thickness of the sample. The IR transmission spectra in the region 400–1600 cm^{-1} for the pure as well as samarium oxide doped glasses were recorded and presented as Fig. 5.

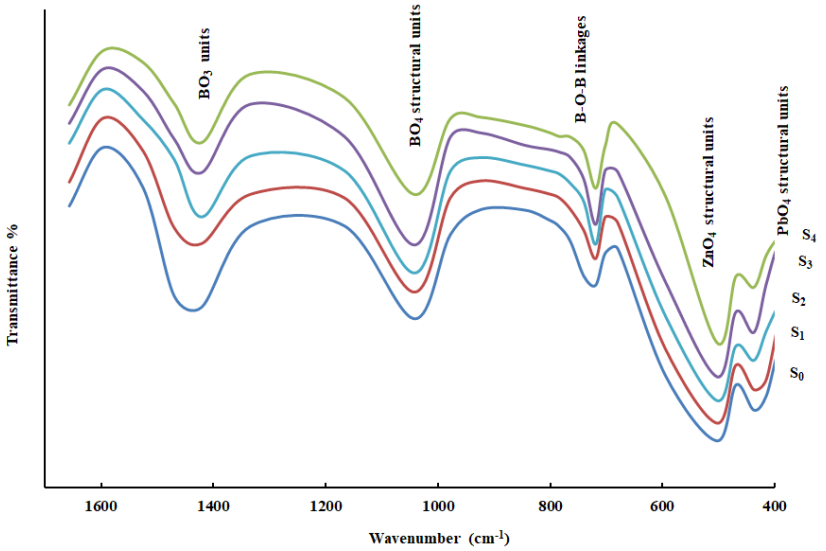

Fig. 5. Fourier transform infrared (FTIR) spectra of ZnF_2–PbO–B_2O_3: Sm_2O_3 glasses

It shows conventional bands due to the presence of borate groups, and they are due to the B–O–B linkages at about 710 cm^{-1}, BO_4 structural units at about 1060 cm^{-1}, BO_3 units are at about 1425 cm^{-1}, respectively. Additionally, at about 450 cm^{-1}, a band due to PbO_4 vibrations is also located in these spectra [13,21]. With the introduction of Sm_2O_3 (0.5–2.0 mol. %) into the glass network, no new additional bands appeared. The summary of the data on various bands observed in the IR spectra of ZnF_2–PbO–B_2O_3: Sm_2O_3 glasses are presented in Table 4.

Table 4. Band positions (in cm^{-1}) in the IR spectra of ZnF_2–PbO–B_2O_3 glasses doped with different concentrations of Sm_2O_3

Assignment	Glass				
	S_0	S_1	S_2	S_3	S_4
BO_3 units, cm^{-1}	1470	1462	1448	1435	1421
BO_4 groups, cm^{-1}	1039	1041	1045	1052	1068
B-O-B linkage, cm^{-1}	719	721	720	719	721
ZnO_4 units, , cm^{-1}	503	503	501	505	502
PbO_4 units, cm^{-1}	437	435	436	442	435
BO_3 units, cm^{-1}	1470	1462	1448	1435	1421

Among different constituents in the present studied glass composition of ZnF_2-PbO-B_2O_3: Sm_2O_3, B_2O_3 is the good glass network former, the primary structural units include; trigonal boron (BO_3) group, tetragonal born (BO_4) group [22], boroxol rings (B_3O_6), when mixed with modifiers, forms a complex super structural unit like di-borate $[B_2O_5]^{2-}$, tri-borate $[B_3O_7]^{5-}$, meta-borate $[BO_2]^-$ and pen-ta-borate $[B_5O_8]^{3-}$etc. The IR transmission spectrum of pure glass sample (S_0) exhibits two groups of characteristic board bands at about 1425 and 1060 cm^{-1}, which are the evidence of trigonal BO_3 and tetragonal BO_4 structural units. Additionally, the spectrum also shows that another two bands at about 710 and 450 cm^{-1} are attributed to the B–O–B vibrations and PbO_4 structural units. The spectrum of sample S_2 also exhibits similar bands with a slight shift in wave number. Further, it is observed that the intensity of the tetragonal BO_4 band increases with the slight shift towards the lower energy side whereas the intensity of the trigonal BO_3 band decreases with a slight shift towards the higher energy side with increasing the content of the samarium ions. The increase in the BO_4 bands by the expensive of the BO_3 band is understood as the addition of the Sm_2O_3 converts the BO_3 units into BO_4 units by introducing the NBOs. This behavior suggests that the samarium ions play a modifier role in the glass matrix when mixed with a small concentration. The decrease in the density of the sample with an increase in the content of Sm_2O_3 also supports the above result as with an increase in the ratio of NBO/BOs, the glass structure becomes loosened and hence the density of the sample decreases with the increase in the content of the samarium ions.

Due to electron-electron coulombic interaction and spin-orbit (LS) coupling interactions among the free ion with $4f^5$ configuration (Sm^{3+} ion) splits into many energy levels specified by typical term symbols. Some major term symbols are ^6H_J(J = 5/2, 7/2, 9/2, 11/2, 13/2, 15/2), ^6F_J (J = 1/2 to 11/2) ^6P_J (J = 3/2, 5/2, 7/2), ^4G_J (J = 5/2, 7/2, 9/2, 11/2), ^4F_J (J = 3/2, 5/2, 7/2, 9/2), ^4I_J (J = 9/2, 11/2, 13/2, 15/2) and ^2H, ^2G, ^2F, ^2P (singlet and doublet states), respectively. By Hund's rule, $^6H_{5/2}$ has lowest $J = |L - S|$) value and is the ground state. When ions, like Sm^{3+}, are placed in a crystal field (like glass or crystals) their energy states split and shift due to the interaction between the ion and the surrounding ions or ligands in the host material. This shifting and splitting depends on the strength of the crystal field and the symmetry of the sm^{3+} ion site in the host. Generally, the absorption bands of the trivalent samarium ions in a host are categorized into two groups low energy transition band group spreads over the wavelength 800–1800 nm, and high energy transition band group spreads over the wavelength 320 to 650 nm. The optical absorption spectra of present investigated samples in Fig. 3 exhibit the sharp intensive bands in the NIR region only and are assigned due to $^6H_{5/2} \rightarrow {}^6F_{11/2}, {}^6F_{9/2}$, $^6F_{7/2}$, $^6F_{5/2}$, $^6F_{3/2}$, and $^6F_{1/2}$transitions respectively. All these transitions are spin allowed (ΔS = 0) and follow ΔJ = 0, ±1 from J = 5/2. The complete disappearance of some absorption transitions due to the presence of the modifier PbO was observed [23] may be due to the factor-like change in local symmetry around Sm^{3+} ions by PbO by reducing cross-linking and introducing NBOs, shielding and quenching effects from Pb^{2+} ions by its heavy atomic cores and high polarizability, interaction between electronic transitions and vibrations (vibronic coupling) succors to forbidden 4f-4f transitions or makes them extremely weak.

Judd-Ofelt (JO) parameters are vital to enhance the comprehension of optical characteristics, particularly concerning rare-earth ions such as samarium in glass

matrices. They bid valuable insights into properties like radiative transition probabilities, oscillator strengths, and branching ratios etc.

By applying JO theory and measuring the area under the absorption curves, the experimental oscillator strengths were determined by the simplified relation [24]:

$$f_{exp} = 4.318 \times 10^{-9} \int \varepsilon(\vartheta) d\vartheta, \quad (3)$$

where $\int \varepsilon(\vartheta) d\vartheta$ is the area under the absorption curve, $\varepsilon(\vartheta)$ is the molar absorptivity of the respective band at ϑ:

$$\varepsilon(\vartheta) = \frac{A}{cl}, \quad (4)$$

where $A/_l$ is the absorbance coefficient, c is the concentration of the lanthanide ion.

The calculated oscillator strengths for the electric dipole transition from the ground state (ψ) to the excited state (ψ') were obtained using the relation:

$$f_{cal} = \left(\frac{8\pi^2 mcv}{3h(2J+1)}\right)\left(\frac{(n^2+2)^2}{9n}\right)\sum_{\lambda=2,4,6}\Omega_\lambda\left(\langle\psi_J||U^\lambda||\psi_{J'}\rangle\right)^2, \quad (5)$$

where all the terms having their own standard meaning, which are mentioned in the literature [25,26], $\|U^\lambda\|$ are the square reduced matrix element of the unit tensor operator of the rank $\lambda = 2, 4, 6$, these standard values were acquired from [27].

The root mean square deviation values from the calculated and experimental oscillator strengths were obtained using the basic relation, which helps to understand the fitment of theoretical data with experimental data in the RE-doped glasses [28]:

$$\sigma_{r.m.s} = \sum \frac{(f_{cal} - f_{exp})^2}{N}. \quad (6)$$

where the absorption band energies (cm^{-1}), the experimental (f_{exp}) and calculated (f_{cal}) oscillator strengths estimated for the absorption band intensities of ZnF_2–PbO–B_2O_3:Sm_2O_3 glasses were presented as Table 5.

Table 5. The absorption band energies and the oscillator strengths for the transitions of Sm^{3+} ions in ZnF_2–PbO–B_2O_3 glasses

Trans. $^6H_{5/2}\rightarrow$		**$^6F_{11/2}$**	**$^6F_{9/2}$**	**$^6F_{7/2}$**	**$^6F_{5/2}$**	**$^6F_{3/2}$**	**$^6F_{15/2}$**	**Root mean square (r.m.s) deviation**
S_1	f_{cal}, 10^{-6}	0.016	4.051	2.554	3.071	2.005	0.324	0.937
	f_{exp}, 10^{-6}	2.250	3.901	2.362	3.164	1.589	0.148	
	Energy ν, cm^{-1}	6390	6781	7279	8115	9254	10586	
S_2	f_{cal}, 10^{-6}	0.015	2.502	2.901	3.319	1.916	0.296	1.521
	f_{exp}, 10^{-6}	3.719	2.409	2.729	3.319	1.590	0.182	
	Energy ν, cm^{-1}	6519	6807	7268	8112	9256	10585	
S_3	f_{cal}, 10^{-6}	0.040	9.689	7.445	8.340	5.078	0.802	2.624
	f_{exp}, 10^{-6}	6.330	9.332	6.922	8.543	4.026	0.373	
	Energy ν, cm^{-1}	6456	6794	7276	8118	9262	10579	
S_4	f_{cal}, 10^{-6}	0.059	15.061	10.796	12.109	7.480	1.193	2.933
	f_{exp}, 10^{-6}	6.998	14.503	1.036	12.41	5.902	1.131	
	Energy ν, cm^{-1}	6419	6774	7272	8118	9262	10579	

Using least squares fitting analysis, JO parameters T_λ $(\lambda = 2, 4, 6)$ were determined with the help of values $\|U^\lambda\|^2$ (taken from the literature), f_{exp}, f_{cal}, and *v* by the relation [29]:

$$f_c = [T_2(\|U^2\|)^2 + T_4(\|U^4\|)^2 + T_6(\|U^6\|)^2]\vartheta. \quad (7)$$

JO Intensity parameters $\Omega_\lambda(\lambda = 2,4,6)$ are calculated from the above obtained T_λ $(\lambda = 2,\ 4,\ 6)$ using the equation:

$$\Omega_\lambda = \left(\frac{3h}{8\pi^2 mc}\right)\left(\frac{9n}{(n^2+2)^2}\right)(2J+1)T_\lambda, \quad (8)$$

where all symbols have their own significant meaning as mentioned in [27], J is taken as 5/2 for the ground state of Sm^{3+} ion. The obtained JO intensity parameters Ω_λ $(\lambda = 2,\ 4,\ 6)$ for Sm_2O_3 doped $ZnO–PbO–B_2O_3$ glasses are displayed in Table 6. When the computed oscillator strengths are compared to the experimental oscillator strengths, a fair match is made. The root mean square (r.m.s) deviation between f_{exp} and f_{calc} is used to express the fit quality. The Judd-Ofelt theory's validity and suitability for the current glasses are confirmed by the comparatively low levels of these deviations.

Table 6. Judd-Ofelt parameters ($\Omega_l \times 10^{-20} cm^2$) of Sm^{3+} doped $ZnF_2–PbO–B_2O_3–B_2O_3$ glasses

Sample	Ω_2	Ω_4	Ω_6	Trends	Ref.
S_1	4.71	2.94	1.83	$\Omega_2 > \Omega_4 > \Omega_6$	This work
S_2	11.6	4.28	2.03	$\Omega_2 > \Omega_4 > \Omega_6$	This work
S_3	24.9	9.41	4.93	$\Omega_2 > \Omega_4 > \Omega_6$	This work
S_4	39.7	13.0	7.21	$\Omega_2 > \Omega_4 > \Omega_6$	This work
LBGS3	9.93	9.84	7.51	$\Omega_2 > \Omega_4 > \Omega_6$	[19]
LTTSm10	1.30	3.08	1.54	$\Omega_4 > \Omega_6 > \Omega_2$	[20]
BLCB20	3.78	0.96	0.68	$\Omega_2 > \Omega_4 > \Omega_6$	[23]

From JO-theory, among Ω_2, Ω_4, Ω_6, the first one is profound to the asymmetry of the local crystal field surrounding the RE-ion by breaking the electric dipole transition selection rule and making them allowed partially, as a result, provides information about the electron sharing behavior (covalent character) between the RE-ion and neighbouring ligands. Hence, the Ω_2 parameter acts like a strain for the asymmetry of the ligand field, reflecting the degree to which the local symmetry is distorted. For all present studied four glasses, the values of W_l are projected primarily in the following sequence: $W_2 > W_4 > W_6$. However, it is also observed that with the increase in concentration of the samarium these W_l (λ =2, 4, 6) increases.

The second phenomenological intensity parameter, W_4 usually describes the strength of electric-dipole transitions between 4f levels of the RE-ions, influenced by medium-range order properties of the host material. The observed increased intensity of the emission band due to electric dipole transition $^4G_{5/2} \rightarrow {}^6H_{7/2}$ along with the increase in W_4 with increasing the concentration of sm^{3+} ions strongly suggests that the local strength around RE-ion is increasing with the surrounding ligand by breaking B-O-B linkages and create NBOs, which may lead the loosening of the glass structure with the enhanced long-range polarization effects. Even though samarium is heavy, with increasing the concentration of Sm^{3+}, its network-modifying role and the structural loosening character can dominate, resulting in lower experimental density and increased molar volume. The observed increase in macroscopic optical properties like molar refraction (R_M) and molar electronic polarizability (α_m) with increasing content of samarium can be expected with increased local asymmetry and covalence around sm^{3+} ion due to a rise in W_2 value and rise in long-range local polarizability of samarium ions with the ligand due to rise in W_4. The observed decrease in the metallization criterion (M) with increasing Sm^{3+} ions also suggests an enhancement in the covalent nature of the glass matrix [30].

The observed increase in the third phenomenological intensity parameter, W_6 with Sm^{3+} content indicates enhanced long- range distortions in the ZnF_2–PbO–B_2O_3 glass matrix, suggests that the network becomes more flexible and polarizable at a broader scale, which, along with increases in W_2 and W_4, supports stronger electric-dipole transitions and enhanced luminescent performance.

To further validate the obtained JO parameters, a comparison with previously reported Sm^{3+} doped glass systems has been carried out and is presented in Table 6. It can be observed that the JO parameters in the present study follow the trend $\Omega_2 > \Omega_4 > \Omega_6$, which is consistent with several borate and oxide glass systems reported in the literature [19,20,23]. The comparatively higher Ω_2 values obtained for the present glasses indicate increased asymmetry and covalent character around the Sm^{3+} ion environment. Such behavior is commonly associated with the formation of non-bridging oxygens and structural modifications induced by rare-earth incorporation in the glass network. The observed values are therefore in reasonable agreement with previously reported results for Sm^{3+} doped glasses.

The favorable optical properties observed for Sm^{3+} doped ZnF_2-PbO-B_2O_3 glasses, including well defined absorption bands, suitable JO parameters and enhanced electronic polarizability, suggest that these materials may serve as promising candidates for photonic applications such as solid-state laser hosts, optical amplifiers, optical sensors and luminescent devices operating in the visible and near-IR regions.

Conclusions

20 % ZnF_2–(20-x) % PbO–60 % B_2O_3:xSm_2O_3 (x = 0, 0.5, 1.0, 1.5, 2.0) glass samples successfully prepared by melt-quenching technique. The amorphous nature of the prepared samples was confirmed by the X-ray diffraction spectra. Various macroscopic physical parameters viz., molar volume, molar refraction, molar electronic polarizability and metallization criterion were estimated using experimental density and refractive index. Optical absorption spectra of sm^{3+}doped samples exhibited intensive sharp bands blended with close convolution due to the vibronic coupling and are identified due to $^6H_{5/2} \rightarrow {}^6F_{11/2}$, $^6F_{9/2}$, $^6F_{7/2}$, $^6F_{5/2}$, $^6F_{3/2}$, and $^6F_{1/2}$ transitions respectively. Using JO-theory, experimental as well as calculated oscillator strengths were evaluated and also identified well in agreement with them. Three phenomenological intensity parameters follow the sequence: $W_2 > W_4 > W_6$. Using these microscopic JO parameters, the behavior of macroscopic optical parameters viz., molar refraction, molar electronic polarizability and metallization criterion were understood. FTIR spectra reveal that Sm^{3+} ions in the present glass matrix play the role of modifier by increasing the ratio of NBO/BOs. Overall, the obtained spectroscopic and structural characteristics indicate that Sm^{3+} doped present glasses are promising materials for photonic applications such as solid-state lasers, optical amplifiers, sensors and luminescent devices operating in the visible and near IR regions.

CRediT authorship contribution statement

Boddu Suresh: experiment and data curation; **Padamati Naresh**: writing – original draft, review & editing; **Pamarthi Sobhanachalam**: investigation; **Nagavarapu Narasimha Rao**: review & editing; **Chatla Rani**: data curation; **Maddireddy Srinivasa Reddy**: supervision.

Conflict of interest

The authors declare that they have no conflict of interest.

References

1. Singh GP, Singh J, Kaur P, Singh T, Kaur R, Singh DP. The role of lead oxide in $PbO-B_2O_3$ glasses for solid state ionic devices. *Materials Physics and Mechanics.* 2021;47(6): 951–961.
2. Misawa M. Structure of vitreous and molten B_2O_3 measured by pulsed neutron total scattering. *J Non-Cryst Solids.* 1990;122(1): 33–40.
3. Alderman OLG. Boroxol ring dissolution in molten and glassy B2O3 by neutron and x-ray diffraction difference methods. *J Chem Phys.* 2025;162(5): 054502.
4. Shirshnev PS, Snezhnaia ZG, Shirshneva-Vaschenko EV, Romanov AE, Bougrov VE. Relation of the optical properties of boron copper-containing glasses on the concentration of lithium. *Materials Physics and Mechanics.* 2018;40(1): 78–83.
5. Klinkov V, Archelkov VB, Semencha AV, Tsimerman EA, Sedegova TY, Rudskoy AI. Halide-containing zinc borosilicate glass as a matrix for $CsPbBr_3$ crystal. *Materials Physics and Mechanics*. 2023;51(2): 27–35.
6. Gautam C, Yadav AK, Singh AK. A Review on Infrared Spectroscopy of Borate Glasses with Effects of Different Additives. To be published in *Int. Sch. Res. Notice.* [Preprint] 2012. Available from: doi.org/10.5402/2012/428497
7. Wright AC. Borate structures: crystalline and vitreous. *Phys. Chem. Glas.: Eur. J. Glass Sci. Technol. B.* 2010;51(1): 1–39.
8. Kamitsos EI, Chryssikos GD. Borate glass structure by Raman and infrared spectroscopies. *J. Mol. Struct.* 1990;247: 1–16.
9. Cheng Y, Xiao H, Guo W, Guo W. Structure and crystallization kinetics of $PbOB_2O_3$ glasses. *Ceram. Int.* 2007;33: 1341.
10. Takaishi T, Ota T, Ogura K, Yoko T. Structural Study of $PbO-B_2O_3$ Glasses by X Ray Diffraction and ^{11}B MAS NMR Techniques. *J. Am. Ceram. Soc.* 2000;83(10): 2543-2548.
11. Dimitrov V, Kim SH, Yoko T, Sakka S. Third harmonic generation in $PbO-SiO_2$ and $PbO-B_2O_3$ glasses. *J. Ceram. Soc. Jpn.* 1993;101(1163): 59–63.
12. Naresh P, Naga Raju G, Reddy MS, Rao TV, Kityk IV, Veeraiah N. Dielectric and spectroscopic features of $ZnO-ZnF_2-B_2O_3$: MoO_3 glass ceramic- a possible material for plasma display panels. *J. Mater. Sci.: Mater. Electron.* 2014;25: 4902–4915.
13. Neeraja K, Rupesh Kumar A, Rao TGV M, Vijayalakshmi P, Rami Reddy M. The spectroscopic properties of Mo^{5+} in $ZnO-ZnF_2-B_2O_3$ glasses. *Trans Indian Ceram Soc.* 2013;72(1): 24–28.
14. Singh D, Singh K, Singh G, Manupriya Mohan S, Arora M, Sharma G. Optical and Structural Properties of $ZnO-PbO-B_2O_3$ and $ZnO-PbO-B_2O_3-SiO_2$ Glasses. *J. Phys.: Condens. Matter.* 2008;20(7): 075228.
15. Singh J, Thakur S, Yadav A, Kumar M. Impact of ZnO on the Physical and Optical Properties of $PbO-B_2O_3$ Glasses. *Acta Phys. Pol. A.* 2022;142: 195.
16. Suresh B, Srinivasa Reddy M, Siva Sesha Reddy A, Gandhi Y, Ravi Kumar V Veeraiah N. Spectroscopic features of Ni^{2+} ion in $PbO-Bi_2O_3-SiO_2$ glass system. *Spectrochim. Acta A.* 2015;141: 263.
17. Saritha D, Markandeya Y, Salagram M, VithalM, Singh A K ,Bhikshamaiah G . Effect of Bi_2O_3 on physical, optical and structural studies of $ZnO-Bi_2O_3-B_2O_3$ glasses. *J. Non-Cryst. Solids.* 2008;354: 5573.
18. Shelby J E, Ruller J. Properties of barium gallium germanate glasses. *Phys. Chem. Glasses.* 198;728: 262.
19. Rajaramakrishna R, Knorr B, Dierolf V, Anavekar R V, Jain H. Spectroscopic properties of Sm^{3+} doped lanthanum borogermanate glass. *J. Lumin.* 2014;156: 192–198.
20. Babu AM, Jamalaiah BC, Sasikala T, Saleem SA, Moorthy LR. Absorption and emission spectral studies of Sm^{3+} doped lead tungstate tellurite glasses. *J Alloys Compd.* 2011;509(14): 4743–4747.

21. Cheng Y, Xiao H, Guo W, Guo W. Structure and Crystallization Kinetics of PbO–B_2O_3 Glasses. *Ceram. Int.* 2007;33(7): 1341.
22. Biradar S, Dinkar A, Bennal AS, Devidas GB, Hareesh BT, Siri MK, Nandan KN, Sayyed MI, Es-soufi H, Chandrashekara MN. Comprehensive investigation of borate-based glasses doped with BaO: An assessment of physical, structural, thermal, optical, and radiation shielding properties. *Opt Mater.* 2024;150: 115176.
23. Srivastava P, Rai SB, Rai DK. Optical properties of Sm3+ doped calibo glass with addition of lead oxide. *Spectrochim. Acta A.* 2004;60(3): 637.
24. Ratnakaram YC, Naidu DT, Kumar AV, Rao JL. Characterization of Tm^{3+} doped mixed alkali borate glasses — spectroscopic investigations. *J Phys Chem Solids.* 2003;64(12): 2487–2495.
25. Judd B R. Optical Absorption Intensities of Rare Earth Ions. *Phys. Rev.* 1962;127: 750.
26. Ofelt GS. Intensities of crystal spectra of rare earth ions. *Journal of Chemical Physics.* 1962;37(3): 511–520.
27. Carnall WT, Crosswhite H, Crosswhite HM. Energy level structure and transition probabilities in the spectra of the trivalent lanthanides in LaF_3. *ANL Rep.* 1978;78: 95.
28. Zhang Y, Liu JM, Liu MH, Zhang ZB, Wong WH, Zhang DL. Error evaluation of Judd–Ofelt spectroscopic analysis. *Spectrochim Acta A Mol Biomol Spectrosc.* 2020;239: 118536.
29. Lakshman S V J, Ratnakaram Y C. Spectral studies of praseodymium(III) and thulium(III) in certain borate glasses. *J. Less-Common Met.* 1986;126: 227.
30. Dimitrov V, Komatsu T. An interpretation of optical properties of oxides and oxide glasses in terms of the electronic polarizability and average single bond strength. *J Univ Chem Technol Metall.* 2010;45(3): 219–250.